Stanford Exploration Project, Report 111, June 9, 2002, pages 253–267

Short Note

Effect of velocity uncertainty on amplitude information

Robert G. Clapp[1]

INTRODUCTION

Risk assessment is a key component to any business decision. Geostatistics has recognized this need and has introduced methods, such as simulation, to attempt to assess uncertainty in their estimates of earth properties (Isaaks and Srivastava, 1989). Geophysics has been slower to recognize this need, as methods which produce a single solution have long been the norm.

The single solution approach has a couple of significant drawbacks. First, since least-squares estimates invert for the minimum energy/variance solution, our models tend to have lower spatial frequency than the true model. Second, it does not provide information on model variability or provide error bars on the model estimate. Geostatisticians have both of these abilities in their repertoire through what they refer to as "multiple realizations" or "stochastic simulations." They introduce a random component, based on properties of the data, such as variance, to their estimation procedure. Each realization's frequency content is more representative of the true model's and by comparing and contrasting the equiprobable realizations, model variability can be assessed. These models are often used for non-linear problems, such as fluid flow. In this approach representative realizations are used as an input to a flow simulator.

In geophysics we have a similar non-linear relationship between velocity and migration amplitudes. Migration amplitudes are used for rock property estimates yet we normally don't assess how velocity uncertainty, and the low frequency nature of our velocity estimates, affect our migration amplitudes. The geostatistical approach is not well suited to answer this question. Our velocity covariance is highly spatially variant, and our velocity estimation problem is non-linear.

In previous works (Clapp, 2000, 2001a,b), I showed how we can modify standard geophysical inverse techniques by adding random noise into the model styling goal to obtain multiple realizations. In this paper I apply this methodology to a conventional velocity analysis problem. I then migrate the data with various velocity realization. I perform Amplitude vs. Angle (AVA) analysis on each migrated image. Finally, I calculate the mean and variance of the AVA parameter estimates for the various relations. In this paper I review the operator based

[1]**email:** bob@sep.stanford.edu

multi-realization methodology. I then apply the methodology on a structural simple 2-D land dataset from Columbia.

MODEL VARIANCE

We can characterize the standard geophysical problem as a linear relationship **L** between a model **m** and **d**, with a regularization operator **A**. In terms of fitting goals this is:

$$\begin{aligned} \mathbf{0} \approx \mathbf{r_d} &= \mathbf{d} - \mathbf{Lm} \\ \mathbf{0} \approx \mathbf{r_m} &= \epsilon \mathbf{Am}. \end{aligned} \tag{1}$$

Ideally **A** should be the inverse model covariance. If so, given an accurate modeling operator we would expect $\mathbf{r_m}$ to be zero. In fact, **A** is an approximation of the inverse model covariance. In practice, we usually assume stationarity, and design **A** to accurately describe the second order statistics of the model. The first order statistics, the spatial variance of the model, are not included. We can produce models that have similar *spatial* variance as the true model by modifying the second goal. This is done by replacing the zero vector **0** with standard normal noise vector η, scaled by some scalar σ_m,

$$\begin{aligned} \mathbf{0} &\approx \mathbf{d} - \mathbf{Lm} \\ \sigma_m \eta &\approx \epsilon \mathbf{Am}. \end{aligned} \tag{2}$$

For the special case of missing data problems, where **L** is simply a masking operator **J** delineating known and unknown points, Claerbout (1998) showed how σ_m can be approximated by first estimated model through the fitting goals in (1). Then, by solving,

$$\sigma_m = \frac{\mathbf{1}'\mathbf{J}\mathbf{r}m^2}{\mathbf{1}'\mathbf{J}\mathbf{1}}, \tag{3}$$

where **1** is a vector composed of 1s. This basically says that we can find the right level of noise by looking at the residual resulting from applying our inverse covariance estimate on known data locations. If we make the assumption that **L** is accurate we can use (3) for a more general case. In the more general case, the operator is 1 at locations where $\mathbf{L}'\mathbf{1}$ is non-zero.

Tomography

The way I formulate my tomography fitting goals requires some deviation from the generic multi-realization form. My tomography fitting goals are fully described in Clapp (2001a). Generally, I relate change in slowness $\Delta\mathbf{s}$, to change in travel time $\Delta\mathbf{t}$ by a linear operator **T** The tomography operator is constructed by linearizing around an initial slowness model $\mathbf{s_0}$. I regularize the slowness **s** rather than change in slowness and obtain the fitting goals,

$$\begin{aligned} \Delta\mathbf{t} &\approx \mathbf{T}\Delta\mathbf{s} \\ \epsilon\mathbf{As_0} &\approx \epsilon\mathbf{A}\Delta\mathbf{s}. \end{aligned} \tag{4}$$

The calculation of σ_d is the same procedure as shown in equation (3). The only difference is now we initiate $\mathbf{r_m}$ with both our random noise component $\sigma_m\eta$ and $\epsilon\mathbf{As_0}$. A cororarly approach for data uncertainty is discussed in Appendix A.

Results

To test the methodology I decided to start with a structurally simple 2-D line from a land dataset from Columbia provided by Ecopetrol. Figure 1 shows the estimated velocity for the data. Note how it is generally $v(z)$ with some deviation, especially in the lower portion of the image. Figure 2 shows the result of performing split-step phase shift migration and Figure 3 shows the resulting angle gathers (Sava, 2000). Note how the image is generally well focused and the gathers with some slight variation below three kilometers at $x = 3.5$. Figure 4 shows the moveout of the gathers in Figure 3. Note the traditional 'W' pattern associated with the velocity anomaly can be seen in cross-section at depth.

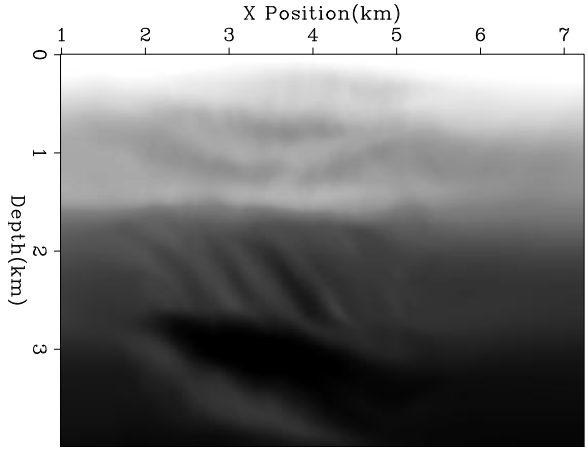

Figure 1: Initial velocity model. bob7-vel-init [CR]

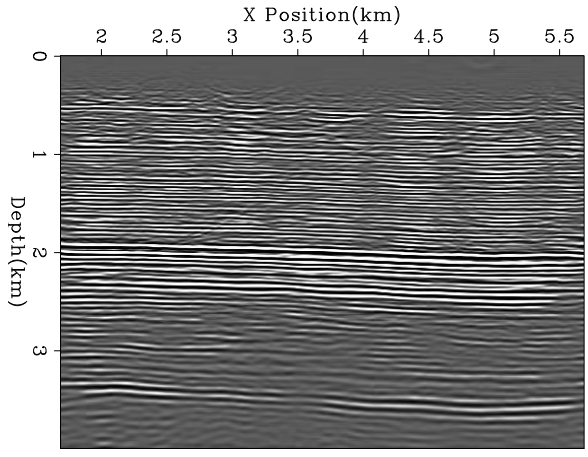

Figure 2: Initial migration using the velocity shown in Figure 1. bob7-image-init [CR]

To start we need to solve the problem without accounting for model variance. If we solve for $\Delta\mathbf{s}$ using fitting goals (4) our updated velocity is shown in Figure 5. The change of the velocity is generally minor, with an increase in the high velocity structure at $x = 3.5$, $z = 3.2$. The resulting image and migration gathers are shown in Figures 6 and 7. The resulting image is slightly better focused below the anomaly and the migration gathers are, as expected, a little flatter. If we apply equation (3) using the $\mathbf{r_n}$ when estimating our improved velocity model we can find the right amount of noise to add to our fitting goals. We can now resolve for $\Delta\mathbf{s}$ accounting for the model variability. Figure 8 shows four such realizations. Note that

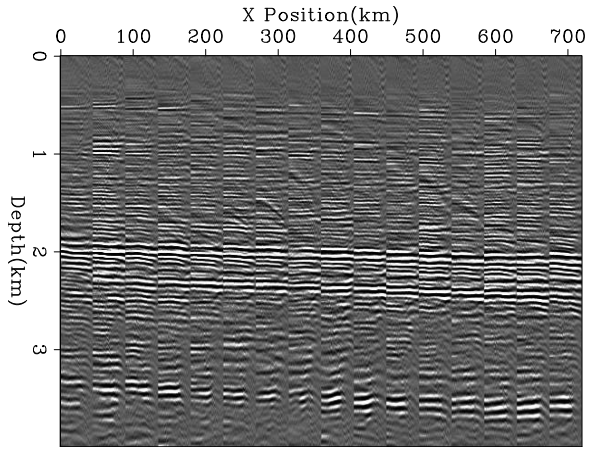

Figure 3: Every 10th migrated gather using the velocity shown in Figure 1. bob7-mig-init [CR]

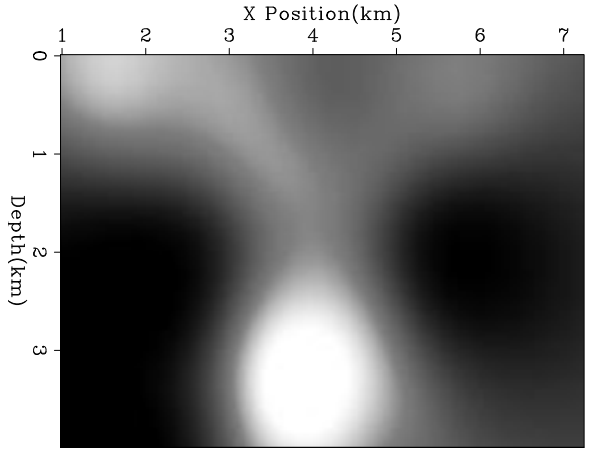

Figure 4: Moveout of the gathers shown in Figure 3. bob7-semb-init [CR]

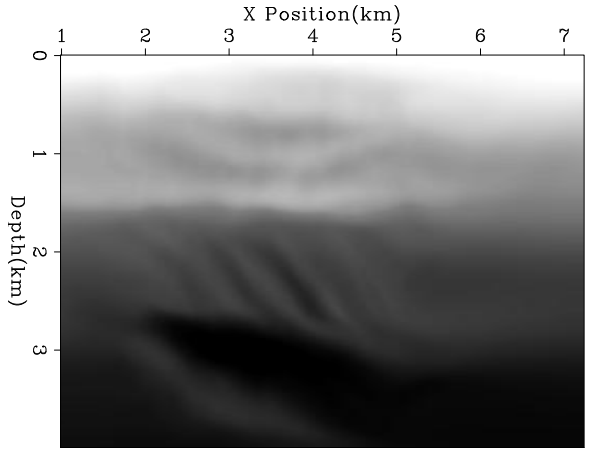

Figure 5: New velocity obtained by inverting for $\Delta\mathbf{s}$ using fitting goals (4). bob7-vel-none [CR]

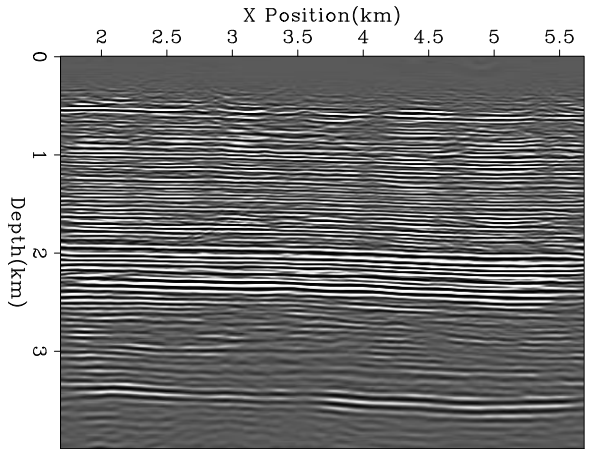

Figure 6: New image obtained by inverting for $\Delta\mathbf{s}$ using fitting goals (4) using the velocity shown in Figure 5. bob7-image-none [CR]

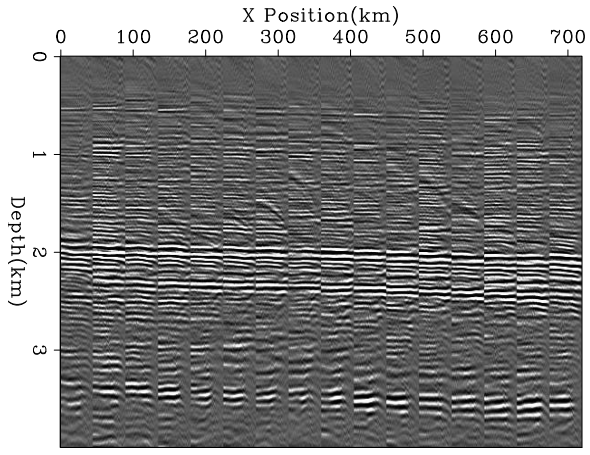

Figure 7: New gathers obtained by inverting for $\Delta\mathbf{s}$ using fitting goals (4) using the velocity shown in Figure 5. bob7-mig-none [CR]

they have the same general structure as seen in Figure 5 but within additional texture that is accounted for by covariance description. If we migrate with these new velocity models we get the images and migrated gathers shown in Figures 9 and 10. In printed form these images appear identical, or close to identical. If watched as a movie, amplitude differences can be observed.

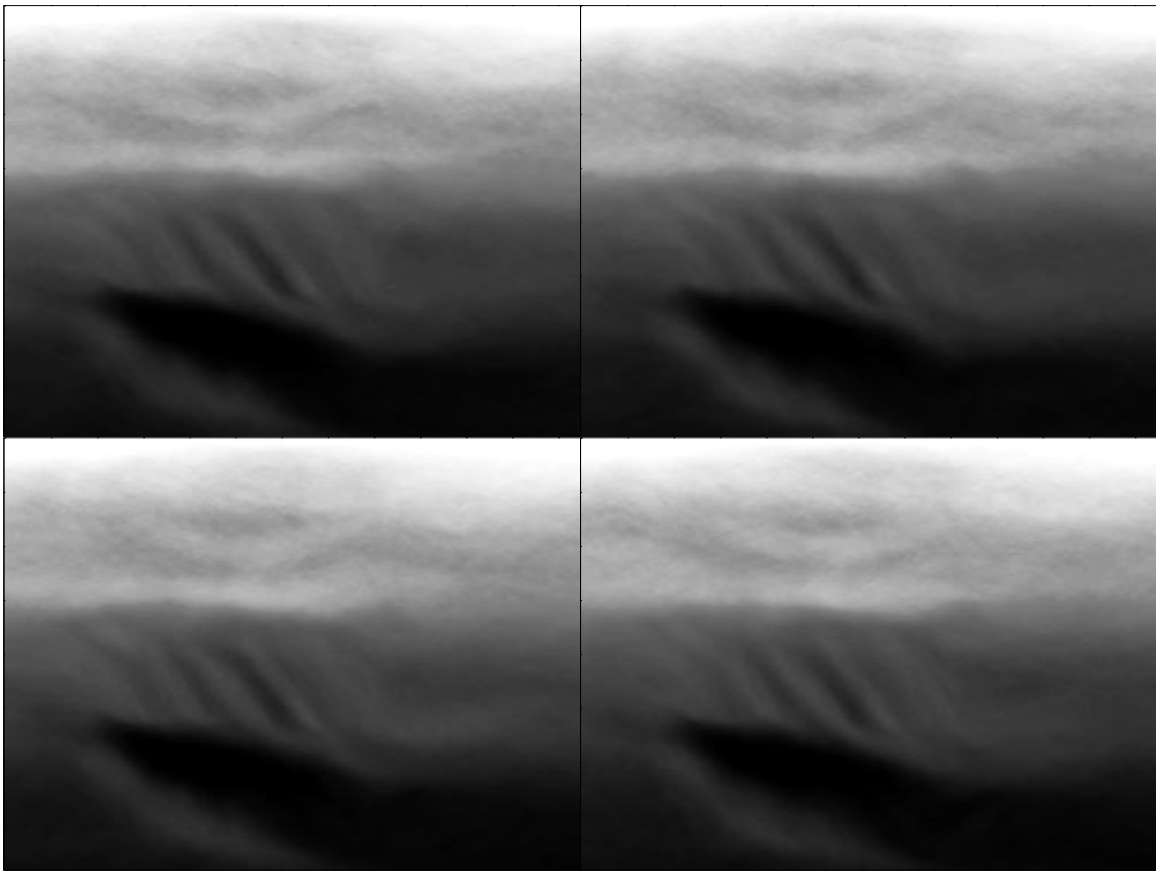

Figure 8: Four different realizations of the velocity accounting for model variability. bob7-vel-multi [CR,M]

AVA analysis

For the AVA analysis I chose the simple slope*intercept (A*B) methodology used in (Castagna et al., 1998; Gratwick, 2001). Figure 11 shows the slope (left), intercept (center), and slope*intercept (right) for the migrated image without model variability. Note the positive, hydrocarbon indicating, anomalies circled at approximately 2.3 km.

I then performed the same procedure on all of the migrated images obtained from the various realizations (Figure 12). The left panel shows intercept, the center panel slope, the right panel, slope*intercept. The top shows the average of the realizations. The center panel shows the variance of the realizations. The bottom panel shows the variance scaled by the inverse of

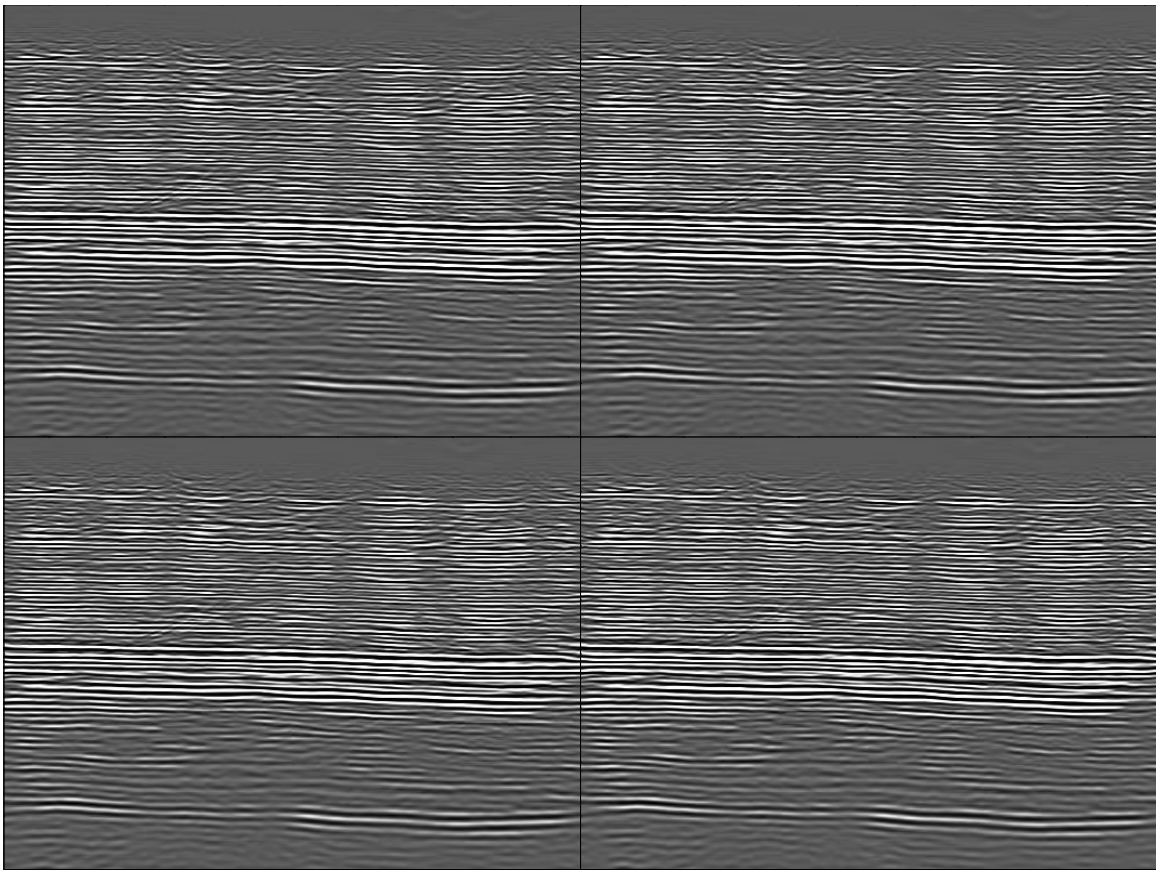

Figure 9: Four different realizations of the migration accounting for model variability. Note how the reflector position is nearly identical in each realization and with the image without variability (Figure 6), but the amplitudes vary slightly. bob7-image-multi [CR,M]

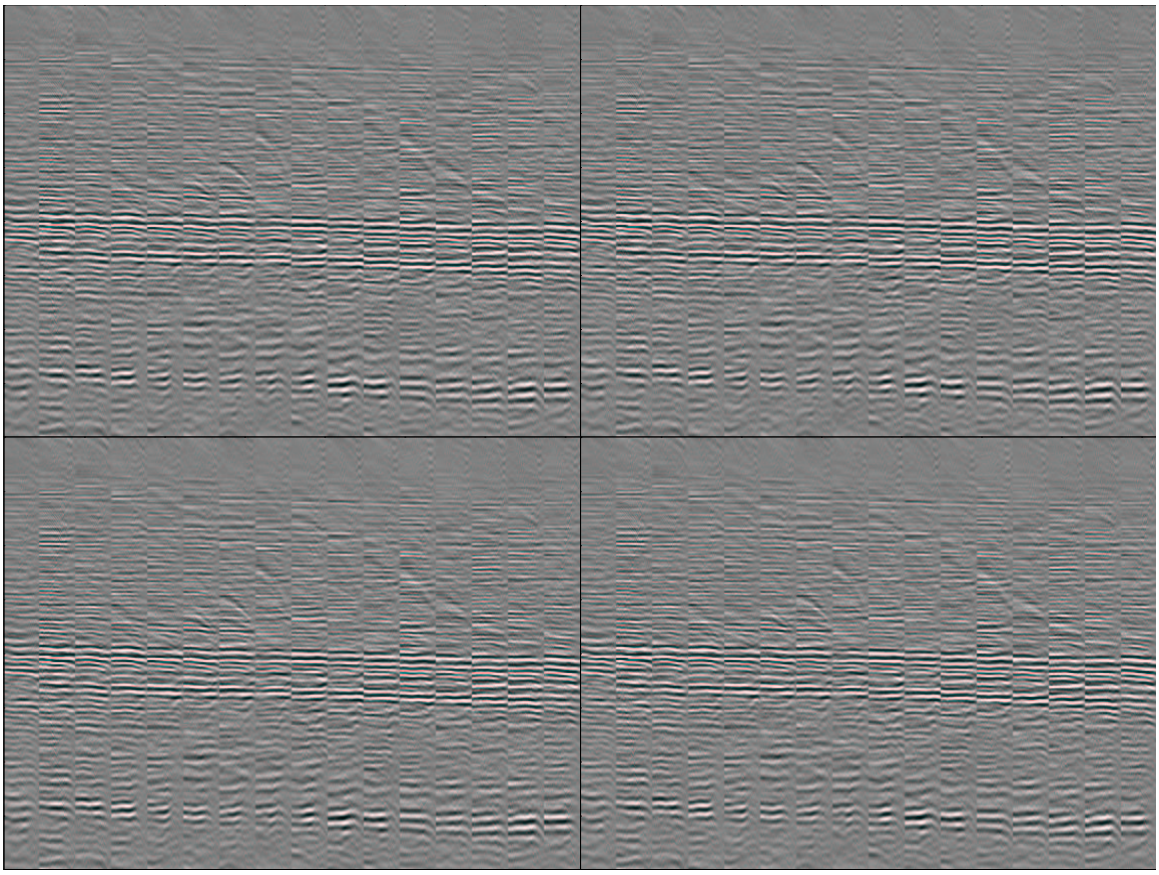

Figure 10: Four different realizations of the migration accounting for model variability. Note how the reflector position is nearly identical in each realization and with the image without variability (Figure 7). bob7-mig-multi [CR,M]

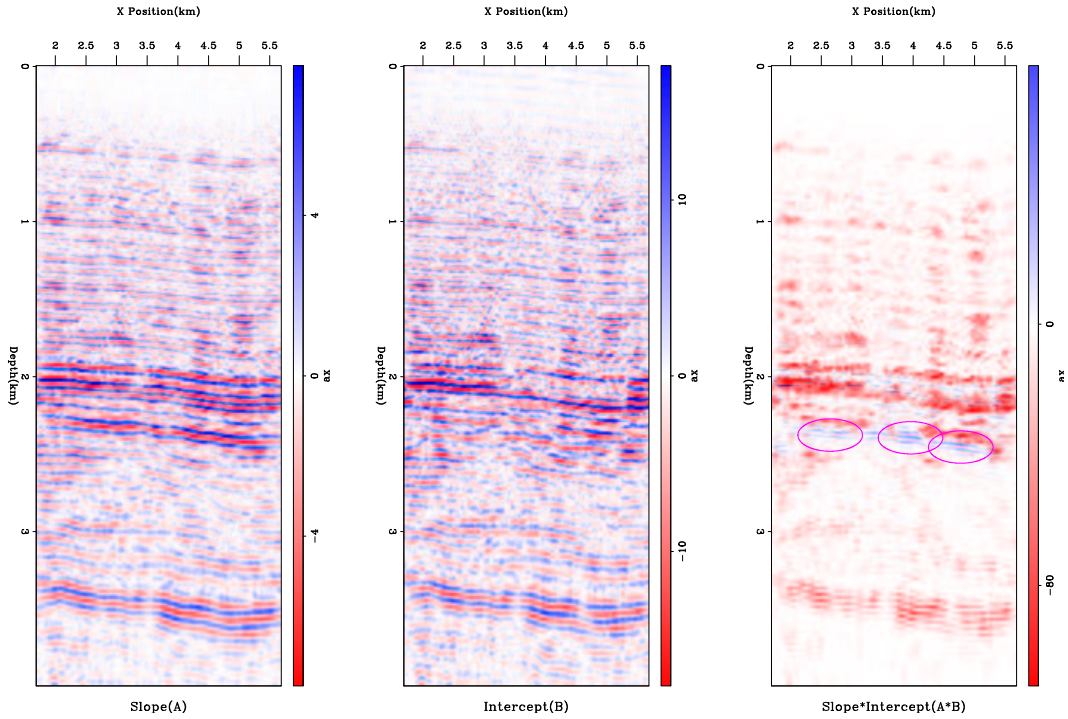

Figure 11: AVA analysis for the migrated image in Figure 7. The left panel shows the slope, the center the intercept, and the right panel the slope*intercept. bob7-ava-none [CR,M]

the smoothed amplitude. What is interesting is the varying behavior at the three zones with hydrocarbon indicators. Figure 13 shows a closeup in the zone with the hydrocarbon indicators. The left blob ‘A’ shows a high variance in the AVA indicator. The center blob ‘B’ shows a mild variance, and the right blob ‘C’ shows low variance. This would seem to indicate that at location ‘C’ the hydrocarbon indicator is more valid. Without drilling of each target a more general conclusion cannot be drawn.

CONCLUSIONS

I showed how AVA parameter variability can be assessed by adding a random component to our fitting goals when estimating velocity. The methodology shows promise in allowing error bars to be placed upon AVA parameter estimates.

ACKNOWLEDGMENTS

I would like to thank Ecopetrol for the data used in this paper.

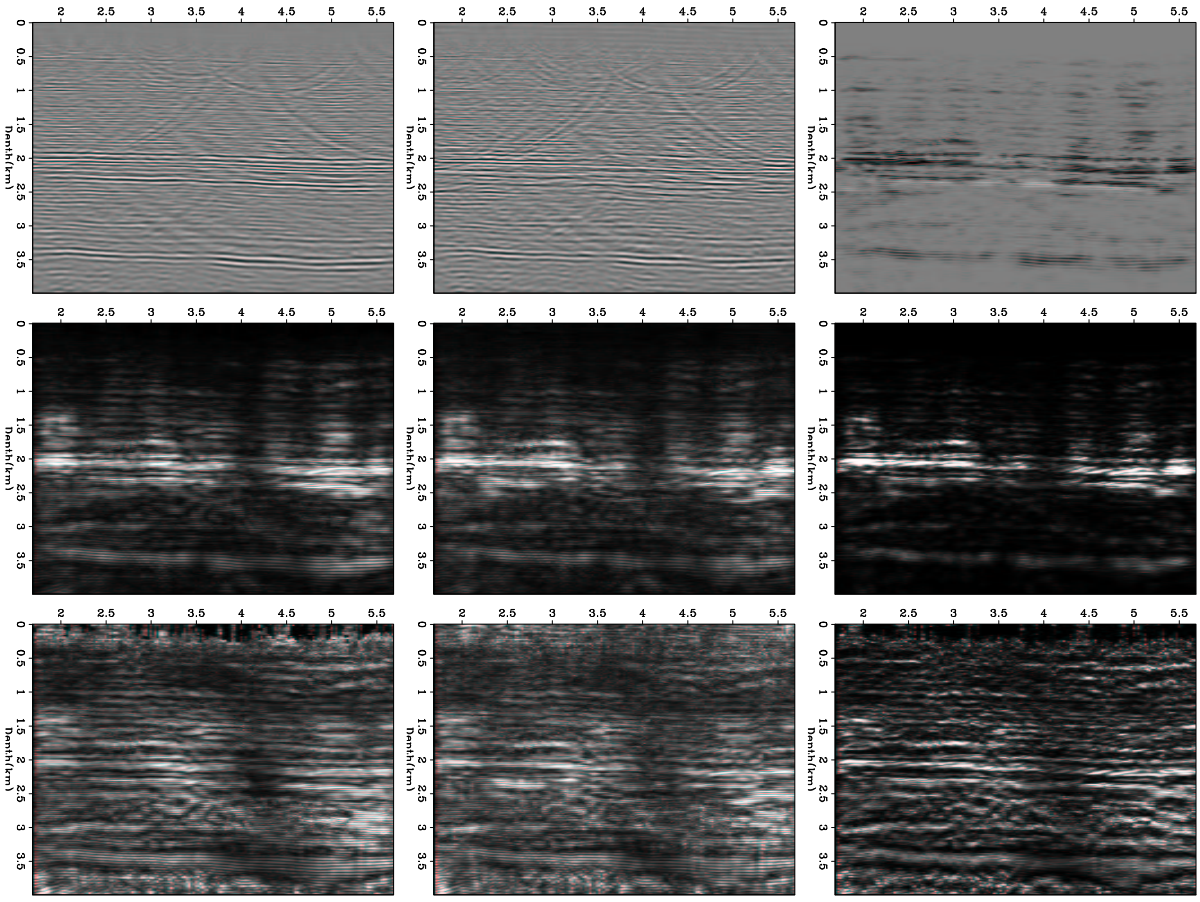

Figure 12: AVA analysis for the the various velocity realizations. The left panel shows intercept, the center panel slope, the right panel, slope*intercept. The top shows the average of the realizations. The center panel shows the variance of the realizations. The bottom panel shows the variance inverse scaled by a smoothed amplitude. bob7-ava-multi [CR,M]

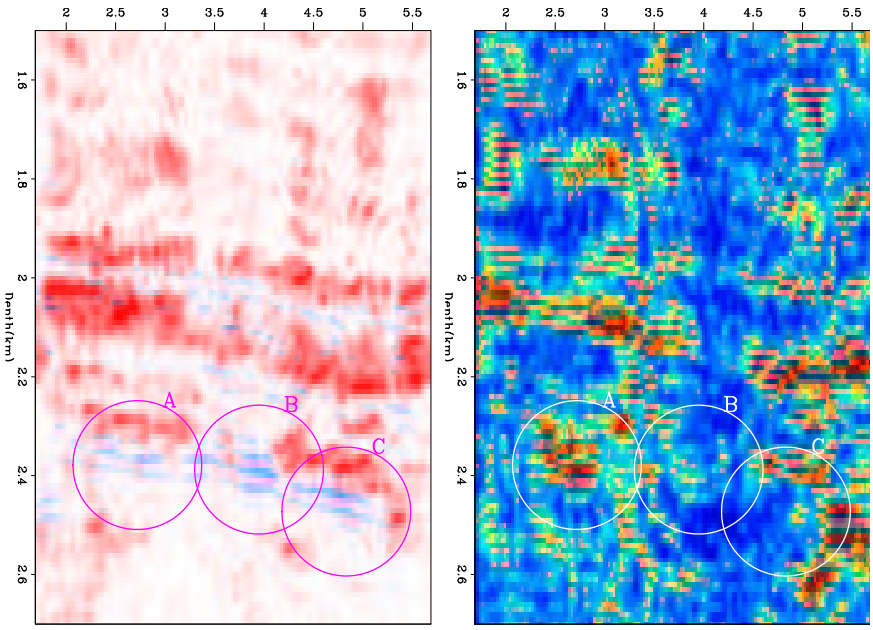

Figure 13: A close up of the reservoir zone. The left panel shows the slope*intercept. The right panel shows the variance of the slope*intercept for the various realizations. Note how the left blob 'A' shows a high variance in the AVA indicator. The center blob 'B' shows a mild variance, and the right blob 'C' shows low variance. bob7-ava-multi-close [CR,M]

REFERENCES

Castagna, J. P., Swan, H. W., and Foster, D. J., 1998, Framework for AVO gradient and intercept interpretation: Geophysics, **63**, no. 3, 948–956.

Claerbout, J. Geophysical Estimation by Example: Environmental soundings image enhancement:. http://sepwww.stanford.edu/sep/prof/, 1998.

Clapp, R., 2000, Multiple realizations using standard inversion techniques: SEP–**105**, 67–78.

Clapp, R. G., 2001a, Geologically constrained migration velocity analysis: Ph.D. thesis, Stanford University.

Clapp, R. G., 2001b, Multiple realizations: Model variance and data uncertainty: SEP–**108**, 147–158.

Gratwick, D., 2001, Amplitude analysis in the angle domain: SEP–**108**, 45–62.

Guitton, A., 2000, Coherent noise attenuation using Inverse Problems and Prediction Error Filters: SEP–**105**, 27–48.

Isaaks, E. H., and Srivastava, R. M., 1989, An Introduction to Applied Geostatistics: Oxford University Press.

Sava, P., 2000, Variable-velocity prestack Stolt residual migration with application to a North Sea dataset: SEP–**103**, 147–157.

APPENDIX A

We can follow a parallel definition for the data fitting goal in terms of the inverse noise covariance **N**:

$$\sigma_d \eta \approx \mathbf{N}(\mathbf{d} - \mathbf{Lm}). \tag{A-1}$$

Noise covariance for velocity estimation

Using the multiple realization methodology for velocity estimation problem posed in the manner results in several difficulties. First, what I would ideally like is a model of the noise. This poses the problem of how to get the noise inverse covariance. The first obstacle is that our data is generally a uniform function of angle θ and a non-uniform function of **x**. What we would really like is a uniform function of just space. We can get this by first removing the angle portion of our data.

I obtain $\Delta\mathbf{t}$ by finding the moveout parameter γ that best describes the moveout in migrated angle gathers. I calculate $\Delta\mathbf{t}$ by mapping my selected γ parameter back into residual moveout and the multiplying by the local velocity. Conversely I can write my fitting goals in terms of $\gamma_\mathbf{i}$ by introducing an operator **S** that maps $\Delta\mathbf{t}$ to γ,

$$\begin{aligned} \gamma_\mathbf{i} &\approx \mathbf{ST}\Delta\mathbf{s} \\ \mathbf{As_0} &\approx \epsilon\mathbf{A}\Delta\mathbf{s}. \end{aligned} \tag{A-2}$$

Making the data a uniform function of space is even easier. I can easily write an operator that maps my irregular $\gamma_\mathbf{i}$ to a regular function of $\gamma_\mathbf{r}$ by a simple inverse interpolation operator **M**. I then obtain a new set of fitting goals,

$$\begin{aligned} \gamma_\mathbf{r} &\approx \mathbf{MST}\Delta\mathbf{s} \\ \mathbf{As_0} &\approx \epsilon\mathbf{A}\Delta\mathbf{s}. \end{aligned} \tag{A-3}$$

On this regular field the noise inverse covariance **N** is easier to get a handle on. We can approximate the noise inverse covariance as a chain of two operators. The first, $\mathbf{N_1}$, f a fairly traditional diagonal operator that amounts for uncertainty in our measurements. For the tomography problem this translate into the width of our semblance blob. For the second operator we can estimate a Prediction Error Filter (PEF) on $\mathbf{r_d}$ (Guitton, 2000) after solving

$$\begin{aligned} \mathbf{0} &\approx \mathbf{r_d} = \mathbf{N_1}(\gamma_\mathbf{r}\mathbf{MST}\Delta\mathbf{s}) \\ \mathbf{As_0} &\approx = \mathbf{r_m}\epsilon\mathbf{A}\Delta\mathbf{s}. \end{aligned} \tag{A-4}$$

If we combine all these points and add in the data variance we get,

$$\begin{aligned} \sigma_d\eta &\approx \mathbf{N_1N_2}(\gamma_\mathbf{r} - \mathbf{MST}\Delta\mathbf{s}) \\ \sigma_m\eta\mathbf{As_0} &\approx \epsilon\mathbf{A}\Delta\mathbf{s}. \end{aligned} \tag{A-5}$$


ST
2100
SOUTH PARK
LONGER & UNCUT